Engineering Innovations
ISSN: 2813-1002, Vol. 12, pp 7-12
doi:10.4028/p-e6xqWP

Submitted: 2023-11-18
Revised: 2024-05-27
Accepted: 2024-05-27
Online: 2025-01-03

Characterization Study of Wire Arc Additive Manufacturing Layer in Metal Inert Gas Welding Process

Muhammad Ivan Fanani[1,a*], Renaldi Candra Saputra[1,b], Aditya Kurnia Putra[1,c], Triyono[1,d]

[1]Department of Mechanical Engineering, Faculty of Engineering
Sebelas Maret University, Indonesia

[a]ivanfanani@student.uns.ac.id, [b]renaldicandrasaputra@student.uns.ac.id, [c]adityaputra05@student.uns.ac.id, [d]triyono74@staff.uns.ac.id

Keywords: WAAM, Corrosion rate, Metallography, ER70S-6, Metal inert gas.

Abstract. The advent of innovative, reasonably priced additive manufacturing techniques has been facilitated by the industry 4.0 era. This study aims to characterize the ER70S-6 wire arc additive manufacturing (WAAM) layer in metal inert gas (MIG) as a result of controlled process speed, electrode type, voltage, and weld current using a three-axis automated motion framework. The study approach begins with the design and building of an automated MIG welding motion system, which includes component manufacture, assembly, calibration, and motion path testing. The specified settings modify the speed of the weld probe motion in response to manual welding parameter adjustments. The investigation continues with the characterization of single to four-layers of WAAM to know the corrosion rate, microstructure, and the Vickers hardness. Corrosion testing results showed that the single-layer of WAAM had the lowest corrosion rate, as well as the highest hardness. Whereas the four-layer had the highest corrosion rate and the lowest hardness.

Introduction

Manufacturing is a process that converts raw resources into finished products. Manufacturing is divided into two categories: conventional manufacturing and modern manufacturing. Conventional manufacturing provides a cost advantage and is more accessible, but it lacks production efficiency. As a result, conventional manufacturing technology must be updated, particularly in modern sectors. Additive manufacturing (AM) is one method for improving conventional manufacturing. This is because AM is versatile, dynamic, and highly adjustable for many industrial applications [1].

AM is a manufacturing process capable of producing parts with complicated geometry for a variety of applications [1]. It can improve product quality without reducing the amount of material used in the machining process. AM can be classed according on the material's usage. Plastic, polymer, and steel are the most prevalent materials used. Wire arc additive manufacturing (WAAM) is a method of AM that produces 3D things by melting wire with an electric arc. The molten wire will be shaped layer by layer until the desired output is achieved [2]. WAAM generally uses three types of machines: MIG (metal inert gas), PAW (plasma arc welding), and TIG (tungsten inert gas) [3].

MIG is one of the WAAM methods that is superior than TIG and PAW. The advantages of the MIG process include the electrode being lured into the torch, the ability to simply change electrode types, and the ability to modify feeding speed. This study seeks to understand the characterization of the WAAM layer in MIG as a result of controlled process speed, electrode type, voltage, and weld current by a three-axis automated motion framework.

Experimental Configuration

The material employed in this investigation was 10xx carbon steel as a substrate, along with argon gas, which is commonly used in welding. The substrate dimensions were 100 mm by 50 mm by 3 mm. The electrode utilized was the ER70S-6 type, with a diameter of 1.0mm. The MIG welding procedure uses electric currents of 100 A. Other parameters, such as the voltage and speed of the three-axis automatic motion framework, will be set to constant values. Electrodes for this study are chosen based on market availability and the existing range that can be utilized to weld thin plates of a given thickness. The WPS (welding process specification) states that the lower current limit for low carbon steel plates with a thickness of 3 mm is 100 A. Welding with a current less than 100 A results in an unsteady arc and low penetration. In contrast, the current limit is 110 A, because welding with a current greater than 110 A causes holes in the plate. The design of this tool is depicted in Fig. 1.

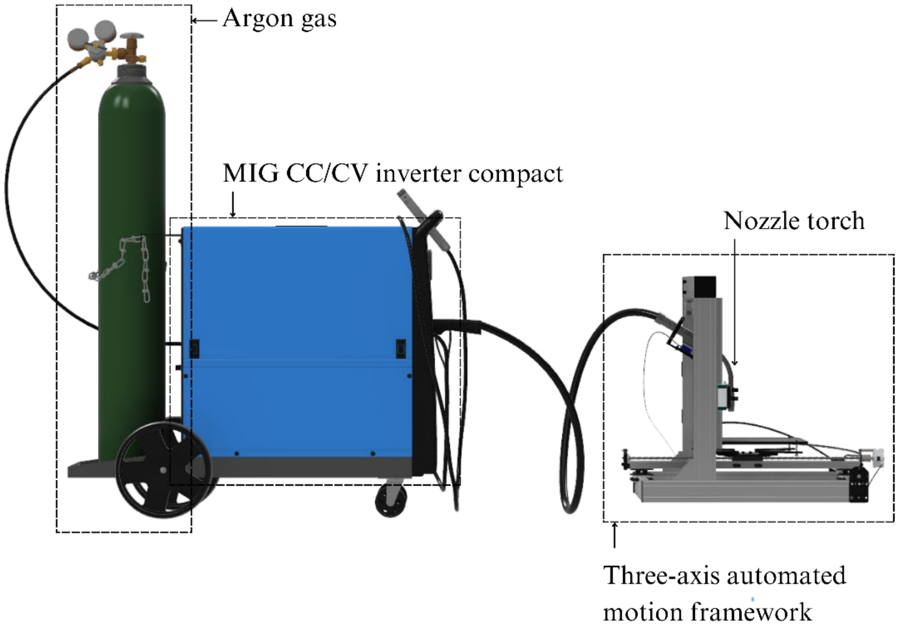

Fig. 1. Wire arc additive manufacturing machine with three axis motion.

The three-axis automated motion framework employed in this study is powered by an electrical arrangement. CAD software is used to create *stl files. Slic3r will decode the *stl file and create a G-Codes file. G-Codes files will be utilized to move the 3D axis with boards that are incorporated into Arduino. The G-codes detected by Arduino will be scanned by the motor driver. The G-Codes will subsequently be sent from the motor driver to the motor stepper. As the desired design input, the lead screw and ball screw will be rotated to produce motion in all three axes.

Prior to specimen fabrication, motion trajectory testing and refining were performed. The tests performed included straight motion tests, rectangle pattern tests, and backslash motion tests. This test makes use of a pen plotter mechanism, in which the pen is inserted and moved along the motion path according to the desired configuration settings. Time and speed measurements were taken during the motion path testing process using manual welding parameters, which were subsequently incorporated into a welding control program.

The WAAM results of one to four layers will be submitted to corrosion testing. This test employed the three-electrode polarization resistance method to test corrosion. Corrosion test performed with CorrTest CS Studio 6.3 software and CorrTest CS350M EIS hardware. The test used a range of -0.25 V to 0.25 V against corrosion potential (E_{corr}) with a scan rate of 10 mV/s. Corrosion testing is performed by scanning V values by rotating the potentiodynamic in stages and obtaining voltage (V) and current (A) data, which are then shown on an E-I graph. From this graph plot yielded Tafel constants for the anode and cathode in the form of graph slope and corrosion current (I_{corr}), which are in the path of the intersection of the two Tafel constants. The corrosion rate is given using the formula:

$$CR = \frac{0.1288\, I_{corr}(EW)}{\rho}. \quad (1)$$

The CR (corrosion rate per year (mpy)) will be translated into millimeters per year (mmpy). In mpyg/μAcm, the constant factor is 0.1288. I_{corr} measures current density in μA/cm^2. ρ is the density in g/cm^3. EW represents equivalent weight (g).

To complete the characterization study, metallographic observations and the Vickers hardness test were used to determine the level of surface hardness in each layer. For depicting how it looks microscopically, a 2% solution of alcoholic nitrid acid was utilized. This experiment was carried out with optical microscope. The Vickers hardness test across the layer was performed on the metallographic specimens using a 500gf load. The formula for the number of hardness is as follows:

$$HV = 1854.4 \times \frac{P}{d^2}. \quad (2)$$

HV is the number of Vickers hardness, 1854.4 is a factor constant, P is the force in gf, d is the indentation's mean diagonal length in μm.

Results and Discussion

Corrosion test uses ASTM G59 standard [4]. This test determines the resistance of materials to oxidation when exposed to an external voltage that causes corrosion. Potential corrosion (E_{corr}) was calculated using the amount of negative charge produced by the metal in a NaCl solution, which creates chloride ions. These ions will harm the metal surface's protective layer (passive film) due to chloride ions infiltrating tiny cavities. Damage to this protective layer is utilized by the oxygen element around it, resulting in corrosion [5]. The corrosion test results are shown in Fig. 2.

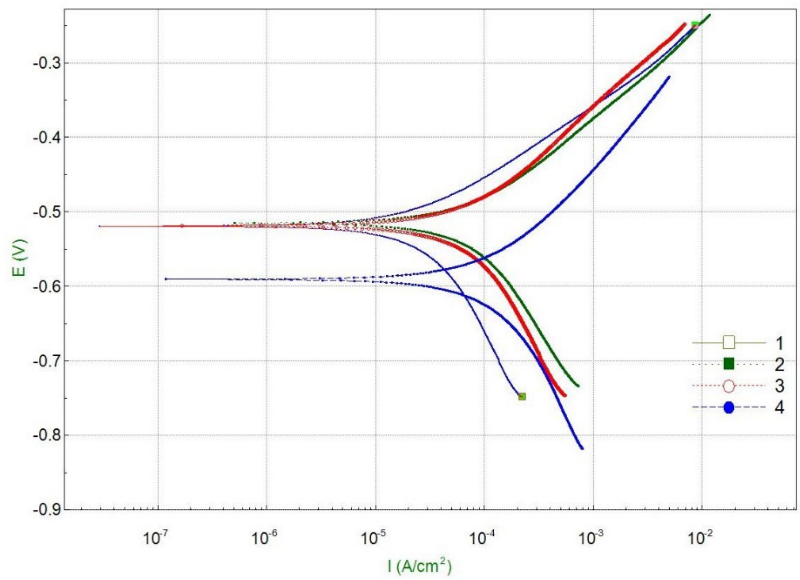

Fig. 2. Corrosion test graph.

Polarization curves appear close together on corrosion test graphs. The discrepancy lies in the values of E_{corr} and I_{corr}, as well as the passivity line. Passivation lines with shapes similar to the anodic and cathodic tangents are more corrosion resistant. The corrosion process is caused by an electrochemical reaction between the specimen's surface and an electrolyte solution. From Fig. 2, we carry out the fitting process to determine the E_{corr} and I_{corr} values so that we can obtain the corrosion rate for each specimen according to formula (1). Those data values are determined by the number of negative charges produced. The size of the number shows the material's tendency to oxidize. The maximum E_{corr}value is achieved when WAAM produces the second layer. A low E_{corr} number will tend to corrode more easily, and vice versa. The corrosion current density was utilized to calculate the corrosion rate desired using the Tafel extrapolation method based on Faraday's law. Corrosion current value (I_{corr}) in the Tafel diagram is affected by the form of the curve since it is calculated from the tangent intersection of the curve that transitions from the cathode to the anode or vice versa. As a result, even though the form is nearly identical, changing the trajectory at a different location produces a different I_{corr}. A different I_{corr} causes a varied corrosion rate [6][7]. Comparison of corrosion rates on each layer producing by WAAM is presented in Fig. 3.

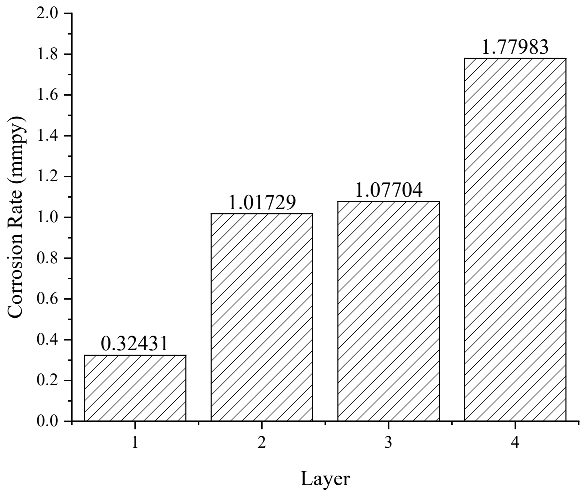

Fig. 3. Corrosion rate result.

According to Fig. 3, the lowest corrosion rate was found in a single layer of WAAM, at 0.32431 mmpy. The corrosion rate gradually increases as more layers are applied. A four-layer WAAM had the highest corrosion rate, measuring 1.77983 mmpy. It is the result of gasses trapped inside the weld metal due to time lag between the creation of a WAAM layer and the next layer, which causes porosity. The more the porosity, the greater the stress concentration, which is the precursor to the production of pitting corrosion [8]. As shown by Fig. 4, ferrite and pearlite dominate the microstructure phase. This observation was conducted in accordance with the ASTM E407 standard [9]. The addition of the WAAM layer results in a less refined microstructure because the cooling rate reduces while grain size increases. The discrepancy in corrosion resistance was attributed to excessive process heat input and an uneven microstructure, which resulted in variances in grain size and element segregation [10].

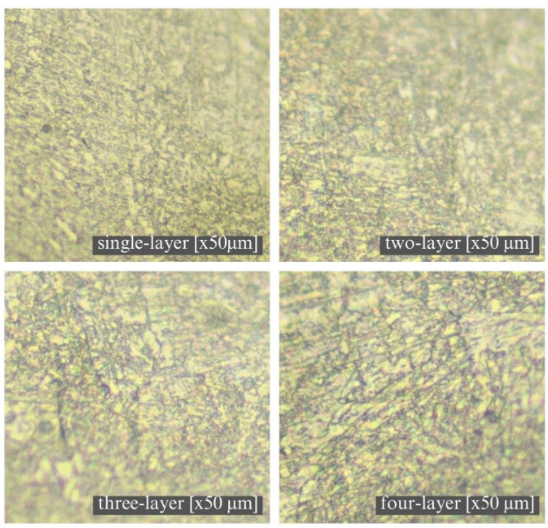

Fig. 4. Microstructure observation result.

Grain size analysis was thus performed on the WAAM material using the micrographs from Fig. 4. Due of the slower cooling rate, which encourages grain growth. Grain size is often found to grow with increasing distance from the substrate; this is owing to slower cooling rates away from the substrate caused by the heatsink effect [11].

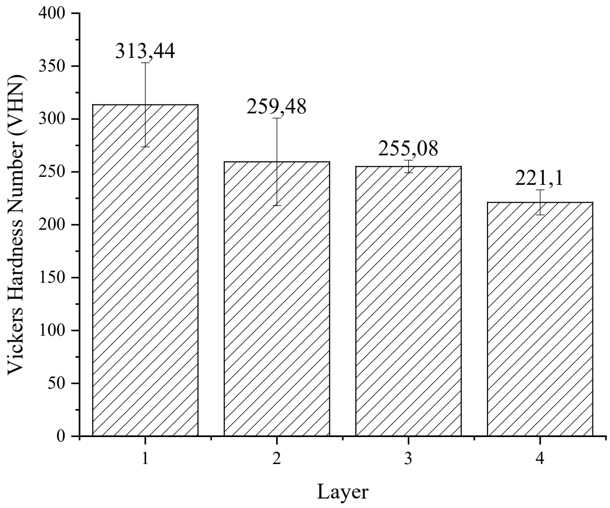

Fig. 5. Vickers hardness test result.

The results of the Vickers hardness test are shown in Fig. 5. This test follows the ASTM E384 standard [12]. The differences in hardness values across WAAM layers are caused by the ferrite density in weld metal [13]. The hardness value decreases with the addition of each subsequent layer. This trend can be attributable to finer grains resulting from rapid cooling [14]. The hardness values increase as the cooling rate rises.

Conclusion

Wire arc additive manufacturing is a type of additive manufacturing that uses melted wire to create three-dimensional objects. By adapting the three-axis automated motion framework for the WAAM layer characterization study, it is possible to deduce that the corrosion rate increases with the layer's addition. Meanwhile, in the hardness value, the reverse phenomena happens, with the addition of the WAAM layer causing it to decrease. This is influenced by grain size changes caused by a decrease in the cooling rate during the WAAM layering process.

References

[1] M.R. Zahidin, F. Yusof, S.H. Abdul Rashid, S. Mansor, S. Raja, M.F. Jamaludin, Y.H. Manurung, M.S. Adenan, N.I. Syahriah Hussein, Research challenges, quality control and monitoring strategy for Wire Arc Additive Manufacturing, J. Mater. Res. Technol. 24 (2023) 2769–2794. https://doi.org/10.1016/j.jmrt.2023.03.200.

[2] C.R. Cunningham, J.M. Flynn, A. Shokrani, V. Dhokia, S.T. Newman, Invited review article: Strategies and processes for high quality wire arc additive manufacturing, Addit. Manuf. 22 (2018) 672–686. https://doi.org/10.1016/j.addma.2018.06.020.

[3] C. Xia, Z. Pan, J. Polden, H. Li, Y. Xu, S. Chen, Y. Zhang, A review on wire arc additive manufacturing: Monitoring, control and a framework of automated system, J. Manuf. Syst. 57 (2020) 31–45. https://doi.org/10.1016/j.jmsy.2020.08.008.

[4] A. International, Standard Test Method for Conducting Potentiodynamic Polarization Resistance Measurements, (2014). https://doi.org/10.1520/G0059-97R14.2.

[5] K. Jones, D.W. Hoeppner, The interaction between pitting corrosion, grain boundaries, and constituent particles during corrosion fatigue of 7075-T6 aluminum alloy, Int. J. Fatigue. 31 (2009) 686–692. https://doi.org/10.1016/j.ijfatigue.2008.03.016.

[6] D.A. Jones, Principles and Prevention of Corrosion, 1996.

[7] S.T. Kim, S.H. Jang, I.S. Lee, Y.S. Park, Effects of solution heat-treatment and nitrogen in shielding gas on the resistance to pitting corrosion of hyper duplex stainless steel welds, Corros. Sci. 53 (2011) 1939–1947. https://doi.org/10.1016/j.corsci.2011.02.013.

[8] N.M.L.P.K. Yasari, N. Muhayat, Triyono, Y.C.N. Saputro, Microstructural and mechanical properties of underwater wet welded SS400 steel, J. Mech. Eng. 5 (2018) 168–179.

[9] A. International, Standard Practice for Microetching Metals and Alloys, (2015).

[10] D.A. Marques, J.P. Oliveira, A.C. Baptista, A Short Review on the Corrosion Behaviour of Wire and Arc Additive Manufactured Materials, Metals (Basel). 13 (2023). https://doi.org/10.3390/met13040641.

[11] C. Huang, P. Kyvelou, R. Zhang, T. Ben Britton, L. Gardner, Mechanical testing and microstructural analysis of wire arc additively manufactured steels, Mater. Des. 216 (2022) 110544. https://doi.org/10.1016/j.matdes.2022.110544.

[12] A. International, Standard Test Method for Microindentation Hardness of Materials, (2022).

[13] R. YIlmaz, M. Tümer, Microstructural studies and impact toughness of dissimilar weldments between AISI 316 L and AH36 steels by FCAW, Int. J. Adv. Manuf. Technol. 67 (2013) 1433–1447. https://doi.org/10.1007/s00170-012-4579-0.

[14] N. Kapustka, C. Conrardy, S. Babu, C. Albright, Effect of GMAW process and material conditions on DP 780 and TRIP 780 welds, Weld. J. (Miami, Fla). 87 (2008) 135–148.